A polarization-independent broadband terahertz absorber

Cheng Shi, XiaoFei Zang, YiQiao Wang, Lin Chen, Bin Cai, and YiMing Zhu

Citation: Applied Physics Letters **105**, 031104 (2014); doi: 10.1063/1.4890617
View online: http://dx.doi.org/10.1063/1.4890617
View Table of Contents: http://scitation.aip.org/content/aip/journal/apl/105/3?ver=pdfcov
Published by the AIP Publishing

A polarization-independent broadband terahertz absorber

Cheng Shi, XiaoFei Zang,[a] YiQiao Wang, Lin Chen, Bin Cai, and YiMing Zhu[a]
Shanghai Key Laboratory of Modern Optical System and Engineering Research Center of Optical Instrument and System, Ministry of Education, University of Shanghai for Science and Technology, Shanghai 200093, China

(Received 25 March 2014; accepted 8 July 2014; published online 21 July 2014)

A highly efficient broadband terahertz absorber is designed, fabricated, and experimentally as well as theoretically evaluated. The absorber comprises a heavily doped silicon substrate and a well-designed two-dimensional grating. Due to the destructive interference of waves and diffraction, the absorber can achieve over 95% absorption in a broad frequency range from 1 to 2 THz and for angles of incidence from 0° to 60°. Such a terahertz absorber is also polarization-independent due to its symmetrical structure. This omnidirectional and broadband absorber have potential applications in anti-reflection coatings, imaging systems, and so on. © *2014 AIP Publishing LLC*.
[http://dx.doi.org/10.1063/1.4890617]

Perfect absorbers are used broadly in thermal detectors,[1] microbolometers,[2] and frequency spectrum imaging systems.[3] The concept of perfect absorbers was first proposed by Landy *et al*. in 2008. In his work, a microwave band perfect absorber was achieved by a three-layer periodic structure.[4] Subsequently, perfect absorbers for microwave,[5] terahertz,[6,7] and infrared[8] bands had been extensively designed and fabricated. Highly efficient absorbers were later explained by the destructive interference between reflected waves from the electrical ring resonator (ERR) and the metallic substrate. Accordingly, non-transmissive, anti-reflective metamaterial devices could be realized by selecting proper ERRs and dielectric spacers.[9,10] However, one single-layer ERR structure is sensitive only to one resonance frequency, resulting in narrowband absorption. To obtain more resonance frequencies, more ERRs with different sizes or shapes are required. Hence, dual band,[11,12] triple band,[13,14] and multi-band absorbers[15,16] were investigated, and broadband functionality was realized through multi-layer ERR structures.[17–19] Broadband absorption can also be realized by using saw-tooth shaped anisotropic metamaterials,[20] surface relief structures,[21] and non-planar structures.[22,23] But these devices with multi-layer structures are complex and difficult either in alignment or in fabrication. On the other hand, absorbers with a simple structure, i.e., heavily doped silicon and metal arrays, were only theoretically proposed.[24,25]

In this Letter, we propose a broadband nearly perfect absorber in terahertz regime, which is simply constructed with a two-dimensional grating and a heavily doped silicon substrate. The absorber is measured by a terahertz time domain spectroscopy (THz-TDS) system[26] and its performances for different angles of incidence are numerically simulated. The results prove that the absorber has a broad absorption bandwidth for a wide range of angles of incidence. Unlike conventional broadband absorbers, the wide absorption spectrum attained in this study is attributed to the perfect combination of destructive interference and diffraction. Furthermore, through our theoretical analyses and numerical simulations, we also find that the absorption spectrum can be tuned by changing the parameters of the structure appropriately. All these characteristics make our absorber have promising prospects.

Such an absorber is realized by etching a grating structure on boron-doped silicon with a resistivity of 0.54 Ω cm, as shown in Fig. 1. This absorber can be divided into two layers: the grating layer (marked as I in Fig. 1(b)) and the substrate layer (marked as II in Fig. 1(b)). According to the Drude model, the complex permittivity of the heavily boron-doped silicon can be represented as[27]

$$\varepsilon = \varepsilon_\infty - \frac{\omega_p^2}{\omega\left(\omega + \frac{j}{\tau}\right)}, \tag{1}$$

where j is the imaginary unit, $\varepsilon_\infty = 11.7$ is the permittivity of the non-doped silicon, τ is the carrier relaxation time, and ω_p

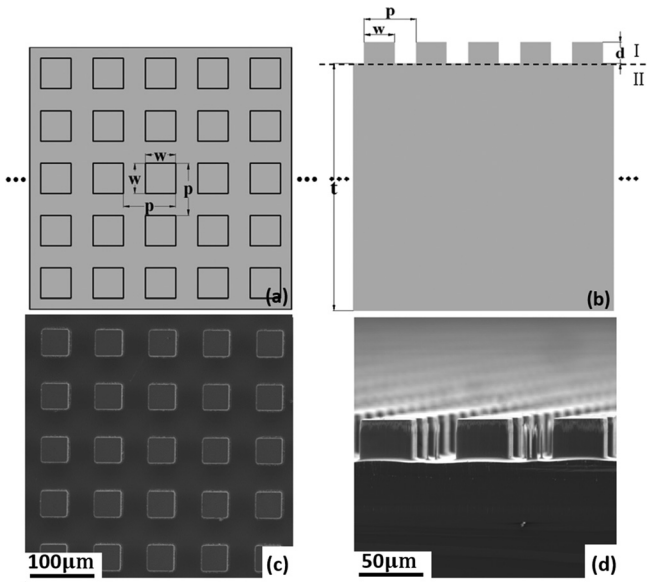

FIG. 1. The structure of the sample: Schematic diagram: (a) top view (b) front view; SEM photograph: (c) top view (d) front view.

[a]Authors to whom correspondence should be addressed. Electronic addresses: xfzang@usst.edu.cn and ymzhu@usst.edu.cn

is the plasma frequency. For a 0.54 Ω cm boron-doped silicon, the corresponding τ is 0.571 ps and ω_p is 19.1 THz.

Here, the transfer matrix method[28,29] is adopted to calculate the transmittance and reflectance of the silicon substrate

$$T = \left| \frac{2}{2\cos(kt) + \frac{j\sin(kt)}{n} + jn\sin(kt)} \right|^2,$$
$$R = \left| \frac{\frac{j\sin(kt)}{n} - jn\sin(kt)}{2\cos(kt) + \frac{j\sin(kt)}{n} + jn\sin(kt)} \right|^2, \quad (2)$$

where t represents the thickness of the substrate, and $k = nk_0$ stands for the wave vector of the electromagnetic wave in the substrate whose refractive index is n. The transmission and reflection spectra for the silicon substrate with different thicknesses are calculated and displayed in Figs. 2(a) and 2(b). The transmission spectra indicate that the transmittance decreases exponentially with the increase of the thickness. More than 99% of terahertz waves cannot propagate through the silicon substrate when the thickness exceeds 300 μm. The reflectance, unlike the transmittance, is independent of the thickness of the substrate and remains approximately 28% from 1 to 2.5 THz. In order to obtain a higher absorption, a grating is added on the silicon substrate to reduce the reflection from it.

To illustrate the anti-reflection mechanisms of the grating in more detail, a simulation of a two-dimensional 0.54 Ω cm boron-doped silicon absorber with $p = 88$ μm, $w = 45$ μm, and $d = 48$ μm is performed via the commercial microwave software CST Microwave Studio® (see Fig. 2(c)). In a low terahertz regime, the grating can be considered as a thin dielectric layer because the wavelength is much longer than the scale of the structure. According to the effective medium theory,[30] the effective permittivity of a one-dimensional grating is calculated as[31]

$$\varepsilon_{//} = (1-r)\varepsilon_{air} + r\varepsilon_{si}, \quad \varepsilon_{\perp} = \frac{\varepsilon_{air}\varepsilon_{si}}{(1-r)\varepsilon_{si} + r\varepsilon_{air}}, \quad (3)$$

where $r = w/p$ is the filling factor of the grating. From Eq. (3), the effective refractive index of a two-dimensional isotropic grating can be calculated as introduced in Ref. 32. Hence, in this situation, the structure of the absorber can be viewed as the heavily doped silicon substrate covered with a thin dielectric film which has a refractive index of n_{eff}. When the terahertz wave impinges on this multi-layer structure, the phase difference of the two reflected waves from the upper and lower surface is equal to $\Delta\varphi = 2n_{eff}d \times 2\pi/\lambda_0$. Destructive interference occurs at the frequency

$$f_i = \frac{(2k+1)c}{4n_{eff}d}, \quad k = 0, 1, 2..... \quad (4)$$

According to Eq. (4), the destructive interference frequency for $k = 0$ is $f_i = 1.17$ THz (see Fig. 2(d)). This coincides with the first reflection dip at $f_1 = 1.17$ THz in the simulation shown in Fig. 2(c).

In a high frequency region, effective medium theory no longer works. The grating should no longer be treated as a dielectric film, but instead as a periodic waveguide array. It is proven by the electric field distribution of the xz plane that the electromagnetic wave is concentrated in the air gap of the grating layer at a high frequency (Fig. 2(f)). The reflectance of the device is known as[33]

$$R = \left|\frac{E_r}{E_i}\right|^2 = \frac{r_1^2 + r_2^2 + 2r_1r_2\cos(2\varphi)}{1 + r_1^2r_2^2 + 2r_1r_2\cos(2\varphi)}, \quad (5)$$

where $r_1 = (Z_{gra} - Z_0)/(Z_{gra} + Z_0)$ is the impedance of the air-grating interface and $r_2 = (Z_{sub} - Z_{gra})/(Z_{sub} + Z_{gra})$ is the impedance of the grating-substrate interface. The reflection can reach a minimum if the matching impedance condition $Z_{gra}{}^2 = Z_0Z_{sub}$ is satisfied. Reference 34 reveals the effective impedance of the grating layer as $Z_{gra} = Z_0(p-w)/p$. Meanwhile, the impedance of the substrate $Z_{sub} = Z_0\cos(\theta_m)/n$ is related to the refractive index n of the substrate, and $\theta_m = \sin^{-1}[m\lambda/(np)]$ is the diffraction angle of the mth order of diffraction. Therefore, the frequency for the matching impedance condition can be stated as

$$f_g = \frac{mc}{\sqrt{n^2p^2 - \frac{n^4(p-w)^4}{p^2}}}, \quad m = 1, 2, 3.... \quad (6)$$

The two-dimensional rigorous coupled-wave analysis (2D-RCWA) method is adopted to analyze the grating diffraction.[35,36] The results (Fig. 2(e)) demonstrate that the [±1,0]-order diffractions play a dominant role from 1.6 THz. For the [±1,0]-order diffractions, the non-reflection frequency of the grating, $f_g = 1.73$ THz, can be calculated from Eq. (6). The CST simulation result also shows that the frequency for the second reflection dip is $f_2 = 1.73$ THz. The

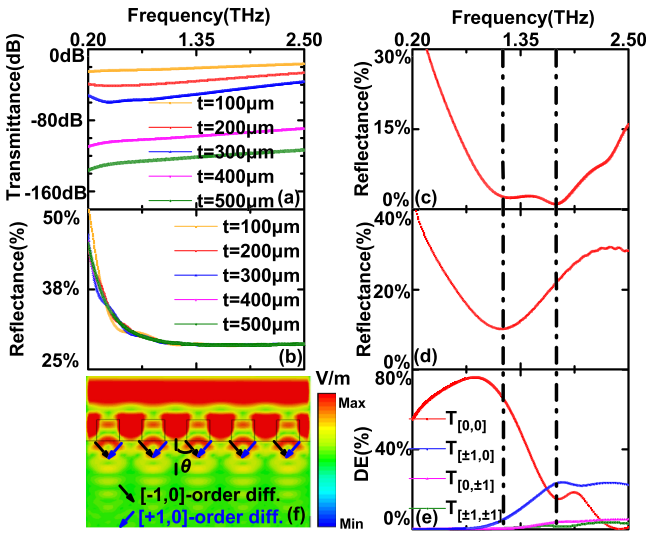

FIG. 2. The result of: (a) The transmission spectra for the substrate with different thicknesses t; (b) The reflection spectra for the substrate with different thicknesses t; (c) The simulated reflection spectrum of the absorber ($w = 45$ μm, $p = 88$ μm, $d = 48$ μm); (d) The calculated reflection spectrum on the basis of the interference by using the effective medium theory (an equivalent layer on the substrate with $d = 48$ μm and $n = n_{eff}$); (e) The diffraction efficiency (DE) of different diffraction orders ($w = 45$ μm, $p = 88$ μm, $d = 48$ μm); (f) The electric field distribution (absolute value) of xz plane for the second reflection dip ($w = 45$ μm, $p = 88$ μm, $d = 48$ μm).

combination of the calculated result from Eq. (6), the 2D-RCWA results and the simulated results prove that the second reflection dip is caused by the diffraction of gratings. Therefore, these two reflection dips will lead to two absorption peaks since the substrate can be regarded as a non-transmissive layer. As mentioned above, destructive interference frequency f_i and non-reflection frequency of the grating, f_g, are related to the structure parameters: w, p, and d. The two absorption peaks can be merged into a broadband absorption spectrum if we adjust these three parameters properly. Numerical simulations are performed to demonstrate the dependence of absorption spectra on these three parameters. Through decreasing the value of p, the red shift of f_i and the blue shift of f_g can be verified by Eqs. (4) and (5), a broader spectrum with lower absorption can thus be achieved (Fig. 3(a)). For the same reason, blue shifts of both absorption peaks can be observed by decreasing the value of w. This can conduce to the blue shift of the absorption spectrum and a narrower absorption bandwidth (Fig. 3(b)). Similarly, as indicated in the equations, d is inversely proportional to f_i but irrelevant to f_g. A smaller value of d means the first absorption peak can be closer to the second one, which will reduce the absorption bandwidth but enhance the absorbance (Fig. 3(c)). We conclude that w mainly controls the frequencies of the absorption peaks, d controls the absorption bandwidth, and p affects both the bandwidth and peaks of the absorption spectrum. Consequently, in order to get a broadband absorption at a designed frequency range, the geometric parameters of the absorber: p, w, d should be adjusted at the same time. Through our optimizations, we chose $w = 45\ \mu$m, $p = 88\ \mu$m, and $d = 42\ \mu$m to make the absorber perform a perfect absorption at a frequency range from 1 THz to 2 THz.

In the experiment, we fabricated the terahertz absorber by utilizing traditional photolithography and the Inductively Coupled Plasma (ICP) etching process on a 0.54 Ω cm p-type silicon wafer. A 1 μm AZP4620 image reversal photoresist layer was spin-coated and patterned by using standard photolithography. By etching for a proper time, the two-dimensional grating structure was formed on the surface of the silicon.

The absorber was measured by a THz-TDS under both transmission and reflection mode. The THz-TDS system works from 0.2 THz to 2.2 THz with a 9.5 GHz spectral resolution. The transmission mode is made up of two pairs of off-axis parabolic mirrors. The first two mirrors are able to focus the terahertz wave on the sample while the other two

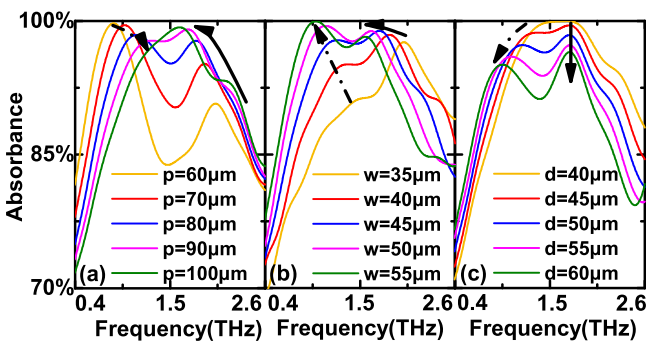

FIG. 3. The dependences of the absorption spectra on: (a) grating depth p; (b) grating width w; (c) grating period d.

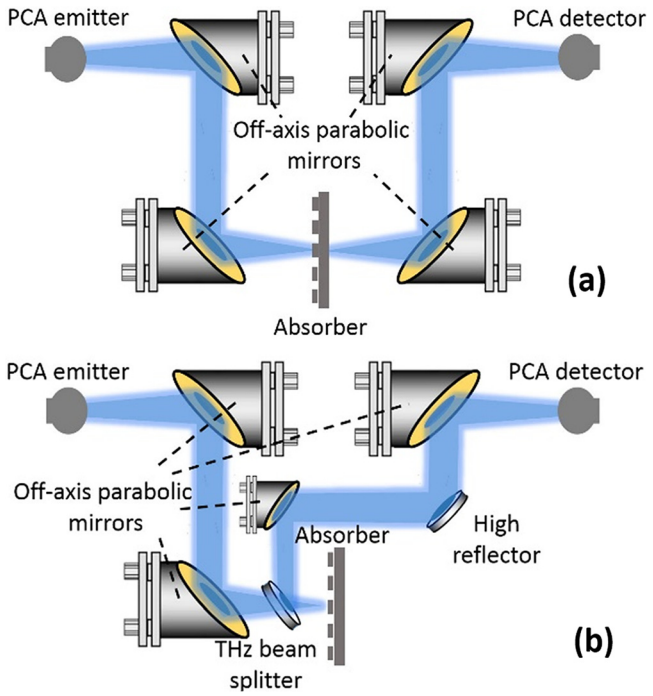

FIG. 4. The THz-TDS system (a) the transmission mode; (b) the reflection mode.

collect the wave and focus it on the detector (Fig. 4(a)). A 50/50 terahertz beam splitter is added to collect the wave reflected from the sample in the reflection mode (Fig. 4(b)). The experimental results verify that the device obstructs the wave propagation and reflection for a broad frequency range (Figs. 5(a) and 5(b)). The absorber can also achieve more than 95% absorption from 1 THz to 2 THz. Since the absorber is 2D symmetrical, it is also insensitive to the polarization states of the incident terahertz waves (Fig. 5(c)). The absorption spectrum of our terahertz absorber using different angles of incidence is also simulated. The absorption can still be greater than 90% for over a 1 THz range, when the angle of incidence is even close to 60° (see Fig. 5(d)).

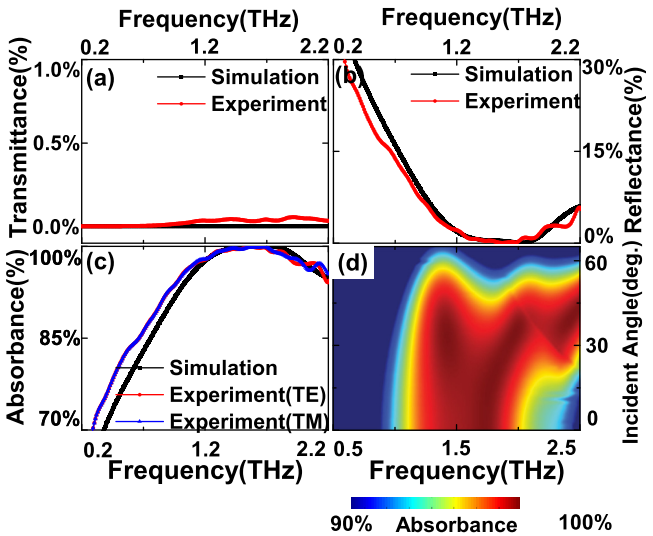

FIG. 5. The simulated and measured results of the polarization independent broadband terahertz absorber with $w = 45\ \mu$m, $p = 88\ \mu$m, $d = 42\ \mu$m: (a) the transmission spectrum; (b) the reflection spectrum; (c) the absorption spectrum; (d) the absorption spectrum for different angles of incidence.

In summary, a very simple and highly efficient broadband terahertz absorber were fabricated by semiconductor process and examined via THz-TDS. The experimental results showed that more than 95% absorption can be obtained from 1 THz to 2 THz. The effective medium theory and the 2D-RCWA method were adopted to explain the mechanisms of the broadband terahertz absorption. We proved that the broadband absorption is caused by the low-transmission substrate and the dual anti-reflection mechanisms of the grating. The simulated results also proved that the absorber could maintain a high absorption with a wide range of angles of incidence. This absorber can have great potential applications in the area of frequency spectrum imaging and so on.

This work was partly supported by National Program on Key Basic Research Project of China (973 Program, 2014CB339806), Basic Research Key Project (12JC1407100), Major National Development Project of Scientific Instrument and Equipment 2011YQ150021 and 2012YQ14000504, National Natural Science Foundation of China (Nos. 11174207, 61138001, 61205094, and 61307126), Shanghai Rising-Star Program (14QA1403100), Program of Shanghai Subject Chief Scientist (14XD1403000), and the Scientific Research Innovation Project of Shanghai Municipal Education Commission (14YZ093).

[1]M. Diem, T. Koschny, and C. M. Soukoulis, Phys. Rev. B **79**(3), 033101 (2009).
[2]N. Liu, M. Mesch, T. Weiss, M. Hentschel, and H. Giessen, Nano Lett. **10**(7), 2342–2348 (2010).
[3]X. Liu, T. Starr, A. F. Starr, and W. J. Padilla, Phys. Rev. Lett. **104**(20), 207403 (2010).
[4]N. I. Landy, S. Sajuyigbe, J. J. Mock, D. R. Smith, and W. J. Padilla, Phys. Rev. Lett. **100**(20), 207402 (2008).
[5]H. Tao, N. I. Landy, C. M. Bingham, X. Zhang, R. D. Averitt, and W. J. Padilla, Opt. Express **16**, 7181–7188 (2008).
[6]H. Tao, C. M. Bingham, D. Pilon, K. Fan, A. C. Strikwerda, D. Shrekenhamer, W. J. Padilla, X. Zhang, and R. D. Averitt, J. Phys. D: Appl. Phys. **43**, 225102 (2010).
[7]F. Ding, Y. Cui, X. Ge, Y. Jin, and S. He, Appl. Phys. Lett. **100**(10), 103506 (2012).
[8]H. Tao, C. M. Bingham, A. C. Strikwerda, D. Pilon, D. Shrekenhamer, N. I. Landy, K. Fan, X. Zhang, W. J. Padilla, and R. D. Averitt, Phys. Rev. B **78**(24), 241103(R) (2008).
[9]H. T. Chen, Opt. Express **20**(7), 7165–7172 (2012).
[10]H. T. Chen, J. Zhou, J. F. O'Hara, F. Chen, A. K. Azad, and A. J. Taylor, Phys. Rev. Lett. **105**, 073901 (2010).
[11]W. Zhu and X. Zhao, J. Opt. Soc. Am. B **26**(12), 2382–2385 (2009).
[12]Y. Ma, Q. Chen, J. Grant, S. C. Saha, A. Khalid, and D. R. S. Cumming, Opt. Lett. **36**(6), 945–947 (2011).
[13]X. Shen, Y. Yang, Y. Zang, J. Gu, J. Han, W. Zhang, and T. J. Cui, Appl. Phys. Lett. **101**, 154102 (2012).
[14]X. Shen, T. J. Cui, J. Zhao, H. F. Ma, W. X. Jiang, and H. Li, Opt. Express **19**(10), 9401–9407 (2011).
[15]Q. Ye, Y. Liu, H. Lin, M. Li, and H. Yang, Appl. Phys. A **107**, 155–160 (2012).
[16]X. Y. Peng, B. Wang, S. Lai, D. H. Zhang, and J. H. Teng, Opt. Express **20**(25), 27756–27765 (2012).
[17]L. Huang, R. D. Chowdhury, S. Ramani, M. T. Reiten, S. Luo, A. J. Taylor, and H. T. Chen, Opt. Lett. **37**(2), 154–156 (2012).
[18]Y. Q. Ye, Y. Jin, and S. He, J. Opt. Soc. Am. B **27**(3), 498–504 (2010).
[19]J. Sun, L. Liu, G. Dong, and J. Zhou, Opt. Express **19**(22), 21155–21162 (2011).
[20]Y. Cui, K. H. Fung, J. Xu, H. Ma, Y. Jin, S. He, and N. X. Fang, Nano Lett. **12**(3), 1443–1447 (2012).
[21]D.-H. Kim, D.-S. Kim, S. Hwang, and J.-H. Jang, Opt. Express **20**(15), 16815–16822 (2012).
[22]D. Ye, Z. Wang, K. Xu, H. Li, J. Huangfu, Z. Wang, and L. Ran, Phys. Rev. Lett. **111**(18), 187402 (2013).
[23]W. Li, T. Wu, W. Wang, J. Guan, and P. Zhai, Appl. Phys. Lett. **104**(2), 022903 (2014).
[24]C. Wu and G. Shvets, Opt. Lett. **37**(3), 308–310 (2012).
[25]M. Pu, M. Wang, C. Hu, C. Huang, Z. Zhao, Y. Wang, and X. Luo, Opt. Express **20**(23), 25513–25519 (2012).
[26]L. Chen, C. Gao, J. Xu, X. Zang, B. Cai, and Y. Zhu, Opt. Lett. **38**, 1379–1381 (2013).
[27]M. V. Exter and D. Grischkowsky, Phys. Rev. B **41**(17), 12140 (1990).
[28]C. C. Katsidis and D. I. Siapkas, Appl. Opt. **41**(19), 3978–3987 (2002).
[29]K. Okamoto, *Fundamentals of Optical Waveguides*, 2nd ed. (Elsevier, Singapore, 2006).
[30]T. C. Choy, *Effective Medium Theory* (Clarendon Press, Oxford, 1999).
[31]D. E. Aspnes, Am. J. Phys. **50**, 704 (1982).
[32]R. Bräuer and O. Bryngdahl, Appl. Opt. **33**, 7875–7882 (1994).
[33]M. Born and E. Wolf, *Principles of Optics*, 7th ed. (Cambridge University Press, Cambridge, 1999).
[34]J. T. Shen, P. B. Catrysse, and S. H. Fan, Phys. Rev. Lett. **94**(19), 197401 (2005).
[35]M. G. Moharam and T. K. Gaylord, J. Opt. Soc. Am. **71**(7), 811–818 (1981).
[36]M. G. Moharam, E. B. Grann, D. A. Pommet, and T. K. Gaylord, J. Opt. Soc. Am. A **12**(5), 1068–1076 (1995).